

International Journal of Robotics and Automation

Volume 26, Issue 2, 2011

Preprint for 206-3458

**“DEVELOPMENT OF A NEW JELLYFISH-TYPE UNDERWATER
MICROROBOT”**

Liwei Shi, Shuxiang Guo, and Kinji Asaka

DEVELOPMENT OF A NEW JELLYFISH-TYPE UNDERWATER MICROROBOT

Liwei Shi,* Shuxiang Guo,*^{**} and Kinji Asaka^{***}

Abstract

Biomimetic microrobots, with multiple degrees of freedom, that can walk and swim smoothly in water are important topics in the field of underwater monitoring for applications such as pollution detection and video mapping. We propose a new type of underwater microrobot using eight ionic polymer metal composite (IPMC) actuators as legs to resolve the problems of asymmetry in previous crawling microrobots. We developed a prototype of this underwater microrobot and conducted experiments to evaluate its walking, rotating, and floating speeds. This microrobot had better performance in walking and rotating than the previous model. Although it achieved its flotation by electrolysing water around the IPMC surface, the electrolysis process was not easy to control. To improve the floating motion, we propose a new jellyfish-type microrobot that moves like a jellyfish when floating and sinking and has four IPMC actuators as legs in place of the jellyfish's antennae. We conducted experiments to analyse the floating motion for three types of bodies and calculated the theoretical floating speeds. We developed a prototype of this jellyfish-type microrobot and evaluated the floating and walking speeds experimentally.

Key Words

Ionic polymer metal composite actuator, jellyfish, biomimetic underwater microrobot, micromechanism

1. Introduction

Biomimetic underwater microrobots, with multiple degrees of freedom (DOF), that can walk and swim smoothly in water or aqueous media are of great interest for underwater monitoring operations including pollution detection, video mapping, exploration of unstructured underwater environments, and other tasks [1, 2]. This kind of microrobot must be simple and compact and must have an efficient system of locomotion. Because the electromagnetic structure of

traditional motors is difficult to shrink, motors are rarely found in this sort of application [3, 4], and special actuator materials are used instead. Significant progress in research into biomimetic microrobots using piezoelectric actuators, shape memory alloy (SMA) actuators, and polymer actuators has been reported [5–7]. However, problems such as electrical leakage, water safety, physical bulk, and high stiffness persist in real applications.

Ionic polymer metal composite (IPMC) is an innovative material made of an ionic polymer membrane chemically plated with gold electrodes on both sides. Its actuation characteristics have significant potential for the propulsion of underwater microrobots. It is light in weight and has a suitable response time, high bending deformation, and long life. Flexible IPMC propulsion blades operating at low driving voltages provide many new possibilities for underwater locomotion applications [26]. They are widely used on soft robotic actuators such as artificial muscles as well as on dynamic sensors [8–15].

Several underwater microrobots have been developed using IPMC and SMA actuators as artificial muscles to propel the robots back and forth. They are widely used in swimming microrobots as oscillating or undulating fins where fast response is required [1, 5, 16–18]. IPMC actuators are also used for underwater bipedal walking microrobots [19–21], and a kind of ion-conducting polymer gel film microleg with two DOF has been developed [22]. In addition, a six-legged insect-inspired underwater walking microrobot has also been described [23]. However, some disadvantages still exist with six-legged devices. The driving forces on the left and right sides are different because of the device's asymmetry. It has difficulty maintaining a straight path when walking forward. Because its centre of gravity and centre of rotation are not the same, it cannot be positioned precisely, and it consumes a lot of energy while rotating. In addition, the six-legged device cannot perform the movements required to dive or surface. With the aim of creating a compact structure with efficient and precise locomotion, we first developed a biomimetic underwater microrobot with eight IPMC actuators as legs to provide better performance in walking and rotating. The eight-legged device floats by electrolysing water around the IPMC surface. However, this electrolysis process cannot be controlled easily. To improve the floating motion, we developed a new jellyfish-type microrobot that mimicked

* Faculty of Engineering, Kagawa University, 2217-20 Hayashi-cho, Takamatsu, Kagawa, Japan; e-mail: s09d504@stmail.eng.kagawa-u.ac.jp, guo@eng.kagawa-u.ac.jp

** College of Automation, Harbin Engineering University, 145 Nantong Street, Harbin, Heilongjiang, China; e-mail: guo@eng.kagawa-u.ac.jp

*** Kansai Research Institute, AIST, 1-8-31 Midorigaoka, Ikeda, Osaka 563, Japan; e-mail: asaka-kinji@aist.go.jp

Recommended by Prof. M.K. Habib

(DOI: 10.2316/Journal.206.2011.2.206-3458)

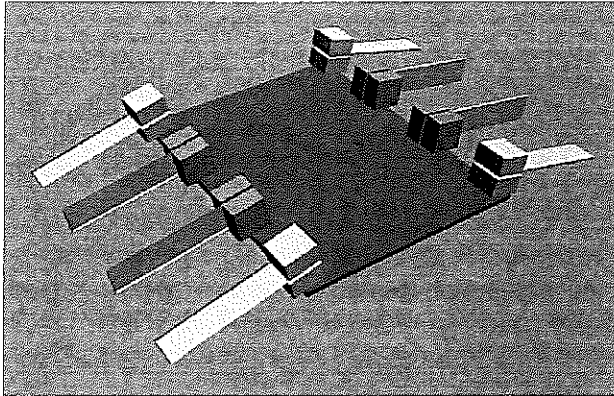


Figure 1. Proposed eight-legged biomimetic microrobot.

the actions of an actual jellyfish when floating and sinking. Four IPMC actuators were used as legs to replace the jellyfish antenna.

The remainder of this paper consists of five parts. First, we describe the design of the biomimetic underwater microrobot with eight IPMC actuator legs shown in Fig. 1, including its walking, rotating, and floating mechanisms. Second, we describe the results of experiments with a prototype of the eight-legged microrobot to measure its walking speed and angular velocity with and without payloads. We also present the results of diving and surfacing experiments conducted using the electrolysis of water around the IPMC surface. Third, we describe a jellyfish-type microrobot designed to improve the floating motion. We analyse three types of microrobot bodies driven by SMA actuators and calculate the theoretical floating speeds. Fourth, we present the results of experiments with a prototype of the jellyfish-type microrobot to evaluate its floating and walking speeds. Last, we present our conclusions.

2. Proposed Eight-Legged Microrobot

2.1 Proposed Eight-Legged Microrobot Structure

Figure 2 shows the structure of the proposed biomimetic microrobot with a centrosymmetric structure around which

the eight legs are symmetrically distributed. It is 33 mm long, 56 mm wide, and 9 mm high. It has eight IPMC actuators designated A through H. Actuators A, B, C, and D are the drivers, and their bending directions are shown in Fig. 3. The other four actuators are supporters. The actuators are all 11 mm long, 3 mm wide, and 0.20 mm thick. The distance between two adjacent drivers or between a driver and a supporter is 10 mm.

The biomimetic microrobot is capable of walking, rotating, and floating. Table 1 lists the control strategies for crawling.

2.2 Crawling Motion Mechanism

The drivers and supporters are driven at the same oscillating frequency. When crawling, the phase of the supporters lags that of the four drivers by 90° . Each step cycle of the walking motion can be separated into four periods as shown in Fig. 4:

1. From d to a , the supporters lift the body up, and the drivers are off the ground.
2. From a to b , the drivers bend forward.
3. From b to c , the supporters bend upward far enough so that they are off the ground, while the drivers in contact with the ground support the body.
4. From c to d , the drivers bend backward in the propulsion stroke, and the body is pushed forward.

During periods 1, 2, and 3, the drivers are off the ground and move to another foothold point with the help of the supporters. In period 4, the drivers push the body forward [7].

The walking speed is determined by the displacement of the drivers and the frequency of the control signal. Because the four drivers are distributed symmetrically on both sides of the structure and they have the same size and mass, the four drivers support equivalent loads and drag forces. Therefore, the four drivers experience the same displacement for the same applied input voltage. The deflections of all the drivers are equal, and they experience the same displacement in each step. The walking speeds on each side of the structure are the same. Suppose that the displacement of the actuator without a payload is d_0 ,

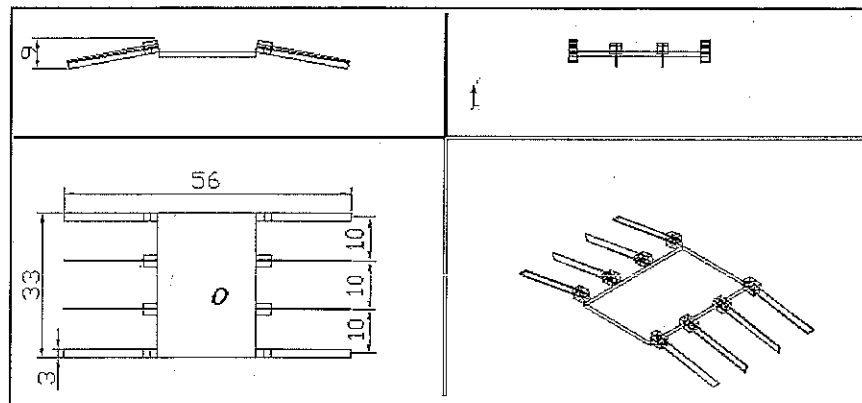


Figure 2. Proposed microrobot structure.

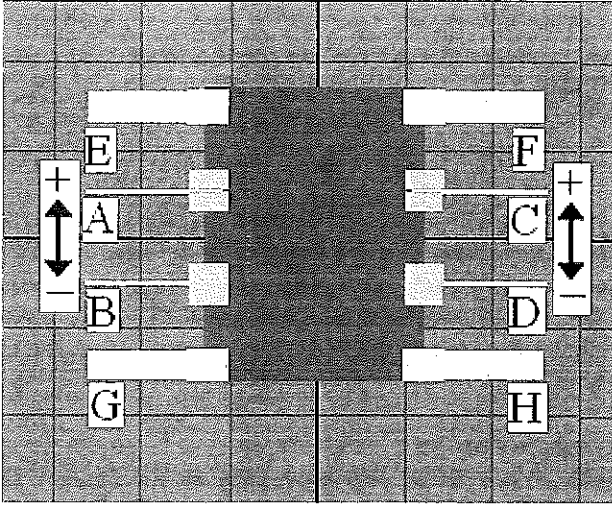


Figure 3. Bending directions for the four drivers.

Table 1
Control Strategies for Crawling Locomotion

Motions	A	B	C	D
Walking forward	+	+	+	+
Walking backward	-	-	-	-
Rotating in clockwise	+	+	-	-
Rotating in counterclockwise	-	-	+	+

A, B, C, and D stand for the drivers, as shown in Fig. 3. "+" and "-" mean the drivers bending forward and backward, respectively.

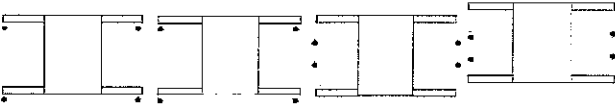


Figure 4. One step cycle of walking forward. The • marks indicate which legs contact the ground.

and the microrobot can move forward with a displacement of d in one step cycle. Because of the payload or water resistance, a decrease Δd in the displacement of the drivers cannot be ignored. Equation (1) describes the relationship between d_0 and d , and (2) describes the walking speed, where v is the average speed and f is the frequency of the input signal:

$$d = d_0 - \Delta d \quad (1)$$

$$v = (d_0 - \Delta d) \times f \quad (2)$$

2.3 Rotating Motion Mechanism and Model

Figure 5 shows the example of counterclockwise rotation. From c to d , the drivers push the body to rotate. In the

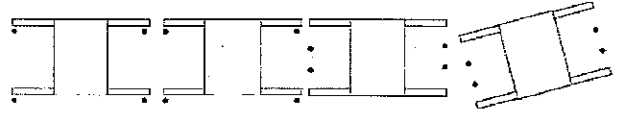


Figure 5. One step cycle of the rotating motion. The • marks indicate which legs contact the ground.

other periods, the drivers are pushed up by the supporters to prepare for the next stroke [14].

The speed of the rotating motion is determined by the angle of the driver in one cycle and the frequency of the step, as shown in Fig. 6(a). The device can rotate by an angle of θ in one step cycle, as shown in (3):

$$\theta = \frac{L}{R} = \frac{2L}{D} \quad (3)$$

Where L is the length of the rotating arc, R is the radius of the rotating rotundity, and D is the diameter, as shown in Fig. 6(a) and (c). The diameter D could be calculated using (4):

$$D = \sqrt{(10 + d)^2 + (56 - 2\Delta l)^2} \quad (4)$$

Where d is the displacement of the driver in the stance phase and Δl stands for the displacement decrease of the IPMC actuator, as shown in (5):

$$\Delta l = l - l_s \quad (5)$$

Where l is the length of IPMC actuator, l and l_s are shown in Fig. 6(b). Based on the geometry theorem, we can get (6):

$$|AN| \times |BN| = |CN| \times |DN| \quad (6)$$

From Fig. 6(b), r is the bending radius of the IPMC actuator, $|AN| = |BN| = l_s$, $|CN| = d/2$, $|DN| = |2r - d/2|$, so l_s can be calculated as shown in (7):

$$l_s = \sqrt{\frac{d}{2} \times \left| 2r - \frac{d}{2} \right|} \quad (7)$$

According to (3), (4), (5), and (7), the device can rotate by an angle of θ in one step cycle, as shown in (8):

$$\theta = \frac{L}{R} = \frac{2L}{D} = \frac{2L}{\sqrt{(10 + d)^2 + \left[56 - 2 \left(l - \sqrt{\frac{d}{2} \cdot \left| 2r - \frac{d}{2} \right|} \right) \right]^2}} \quad (8)$$

Equation (9) gives the rotating speed. Here, because the rotating arc $L \approx d$, we can approximate L by d in (9). The ω and f are the rotating speed and the frequency, respectively. Figure 6(a) shows that the structure's centre of rotation is at point O , which is also the structure's centre

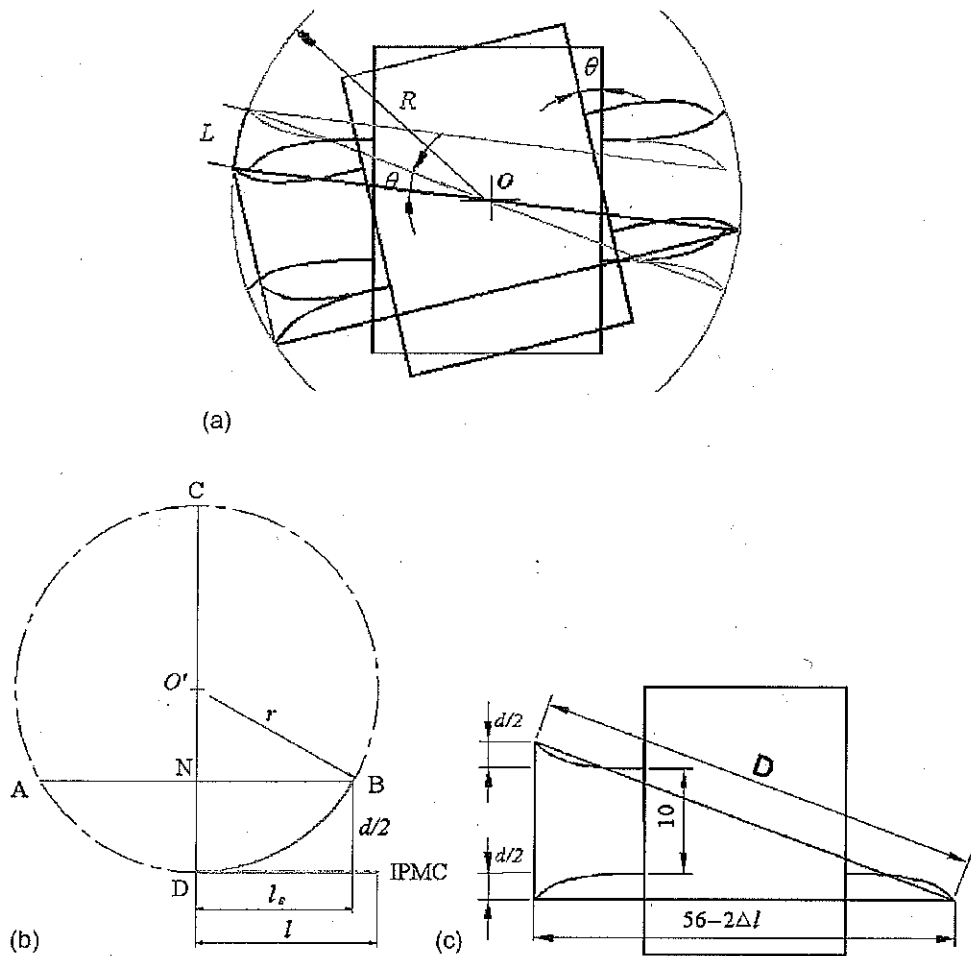


Figure 6. Efficiency of the driver during rotating motion.

of symmetry. Because the eight legs are symmetrically distributed around the centre of symmetry of the centrosymmetric structure and because the eight legs have the same size and mass, the centre of symmetry is also the centre of gravity. Thus, the centre of rotation of the microrobot is its centre of gravity. In addition, because the oscillating directions of the four drivers are close to perpendicular to the radius of rotation, the eight-legged device has a larger torsion angle than the previous six-legged version:

$$\omega = \theta * f = \frac{2(d_0 - \Delta d)}{\sqrt{(10 + d)^2 + \left[56 - 2 \left(l - \sqrt{\frac{d}{2}} \cdot \left|2r - \frac{d}{2}\right|\right)\right]^2}} f \quad (9)$$

2.4 Floating Motion Mechanism

The water around the surface of the IPMC actuators is electrolysed by decreasing the frequency of the applied voltage to 0.3 Hz. The buoyancy of the microrobot can be controlled by the resulting change in volume to make it float upwards, remain neutrally buoyant, or sink downwards. Table 2 lists the control strategies for the floating motion.

Table 2
Control Strategies of Floating Locomotion

Conditions	Floating Motions
$\rho g(V + \Delta V) < mg$	Sinking downward
$\rho g(V + \Delta V) = mg$	Suspended
$\rho g(V + \Delta V) > mg$	Floating upward

ρ is the density of water, g is the acceleration of gravity, V is the volume of the microrobot, ΔV is the volume of the bubbles, and mg is the weight of the microrobot.

3. Prototype Microrobot and Experiments

3.1 Prototype Eight-Legged Microrobot

Figure 7 shows the prototype of the eight-legged microrobot. It has eight actuators fixed on a film body with wood clips. The control signals are transmitted by enamel-covered wires 300 mm long with a copper diameter of 0.03 mm. The wires are soft enough that the resistance can be ignored.

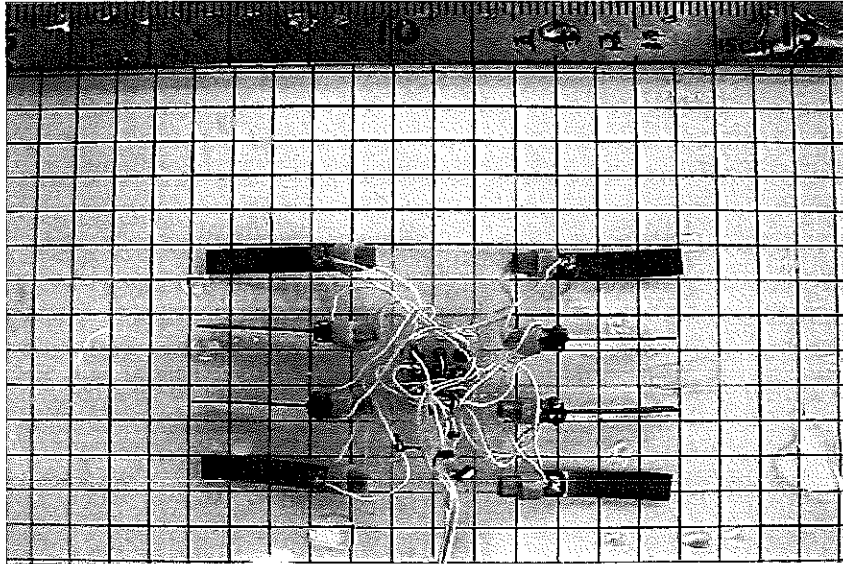


Figure 7. Prototype eight-legged underwater microrobot.

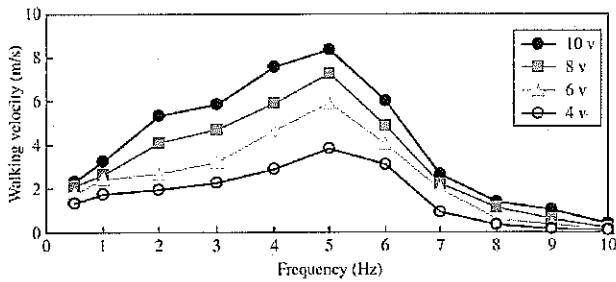


Figure 8. Experimental speed results during walking.

3.2 Walking Experiment without Payload on Underwater Flat Surface

To evaluate walking locomotion, we carried out an experiment on an underwater plastic surface. We recorded the times required to walk a distance of 50 mm using different applied signal voltages and frequencies. The experiment was repeated 10 times for every set of control signals to determine the average speed on the flat surface. The experimental results described in Fig. 8 show that the walking speed was nearly proportional to the input voltage, and a top speed of 8.3 mm/s was obtained with a control signal of 10 V and 5 Hz.

3.3 Rotating Experiment without Payload on Underwater Flat Surface

We also investigated the rotating motion on the same underwater plastic surface. We recorded the times for rotating through 90° under the influence of different voltages and frequencies of the control signal, and calculated the average angular velocity for 10 repetitions of the same experiment. The experimental results described in Fig. 9

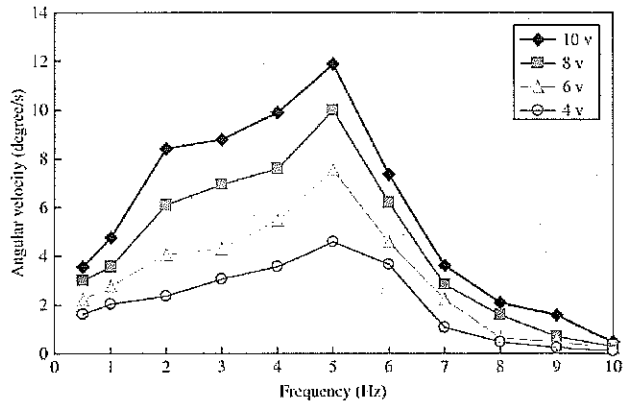


Figure 9. Experimental angular velocity results during rotation.

show that the angular velocity was nearly proportional to the input voltage, and a top angular rotation speed of 11.86°/s was obtained for a voltage of 10 V and a frequency of 5 Hz.

3.4 Walking Experiment with Payload on Underwater Flat Surface

We applied payloads to the structure and conducted walking experiments as shown in Fig. 10 to evaluate the load-carrying ability of the microrobot. The experimental conditions were the same as the experiments without payloads. Figure 11 shows the walking speeds with payloads. The maximum payload was about 4 g.

3.5 Floating Experiment

To test floating locomotion, we set the frequency of the applied voltage to 0.15 Hz to electrolyse the water around

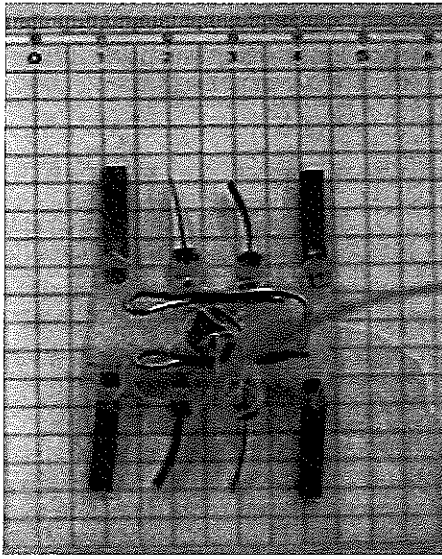


Figure 10. Walking experiment with a 2-g payload.

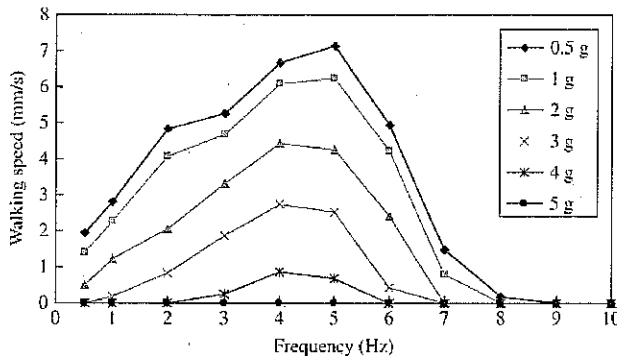


Figure 11. Experimental speed results with payloads during walking.

the IPMC surface. When the input voltage was cut off while the microrobot was floating upward, the microrobot gradually stopped moving upward and then started to sink. The maximum upward floating speed was 4 mm/s with a voltage of 10 V as shown in Fig. 12.

4. Jellyfish-Type Underwater Microrobot

4.1 Jellyfish-Type Microrobot Structure

The eight-legged underwater microrobot used the electrolysis of water on the surface of the IPMC actuators to float; however, controlling the buoyancy is difficult using this method. If the voltage is cut off while the microrobot is floating upward, the gas still attached to the surface of the actuator keeps it moving upward for some time, so it does not immediately stop moving or sink, and the vertical motion cannot be easily controlled. We propose the jellyfish-type microrobot shown in Fig. 13 to achieve both a compact structure and efficient locomotion. This

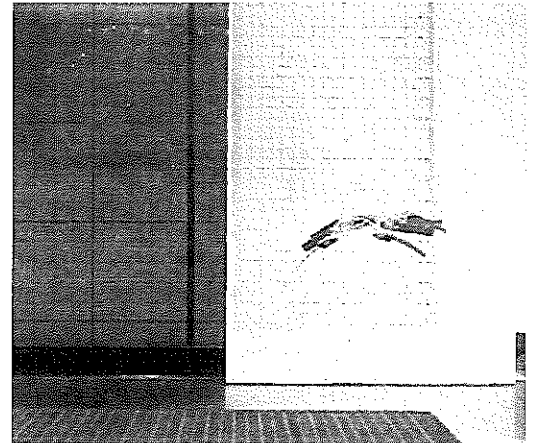


Figure 12. Floating motion of the eight-legged microrobot.

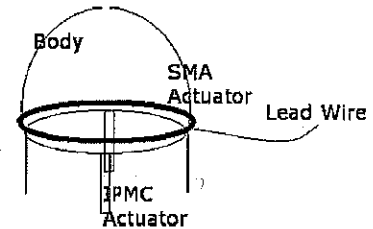


Figure 13. Structure of the jellyfish-type microrobot.

microrobot consists of a body, four legs, an SMA actuator, and control wires. The hemispherical body is made of a rubber material that encloses the sealed SMA actuator. The four legs are driven by IPMC actuators. The microrobot is capable of walking and floating motions.

4.2 Three Body Types

We designed the body to imitate a jellyfish to overcome the problems with floating and sinking experienced by the previous prototype. In this version, the body shrinks when the voltage is applied to its ends. The volume of the body is reduced and the water in the body is squeezed out. This changes the buoyancy and produces an upward force. The body floats upward when the force reaches a certain value. The upward force can be changed by controlling the frequency of the actuator shrinkage and the voltage between its two ends. This means that the microrobot can be made to float upwards, be neutrally buoyant or sink as required. We used three kinds of bodies developed in previous research: a ring type, spiral type, and two-ring type as shown in Fig. 14.

4.3 Characteristic Measurement of the Three Bodies

Using the principle of hydrodynamics, we can calculate the relative speed of the body and the water expelled from the

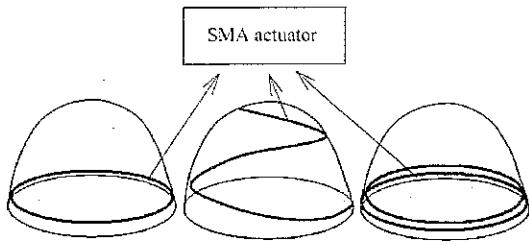


Figure 14. Three types of bodies of the jellyfish-type microrobot.

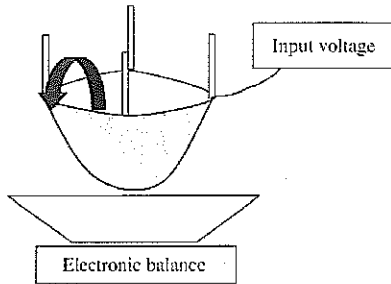


Figure 15. System for measuring the average volume change.

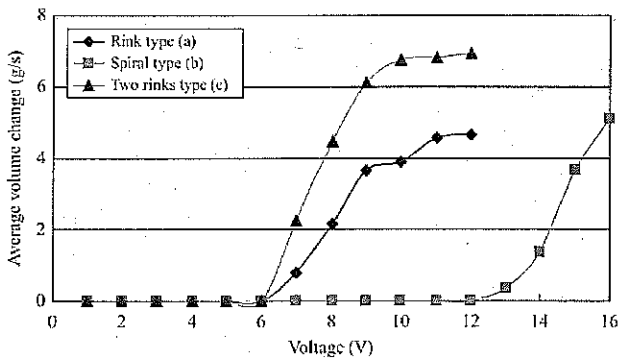


Figure 16. Average volume change for three types of bodies.

body as shown in (10), where Q is the average volume of the water expelled per second, and A is the area of the cross section.

The average weight of water expelled per second can be measured by the system shown in Fig. 15. First, the body filled with water is placed on an electronic balance. Under the influence of different applied voltages, the SMA actuator in the body begins to shrink, and the water is squeezed out of the body. We can calculate the average weight of water expelled per second by recording the time and the value from the electronic balance. Figure 16 shows the experimental results for the three types of bodies. The two-ring type of body had the largest volume change per second for the same input voltage. The spiral type of body required a higher input voltage to shrink, even though its

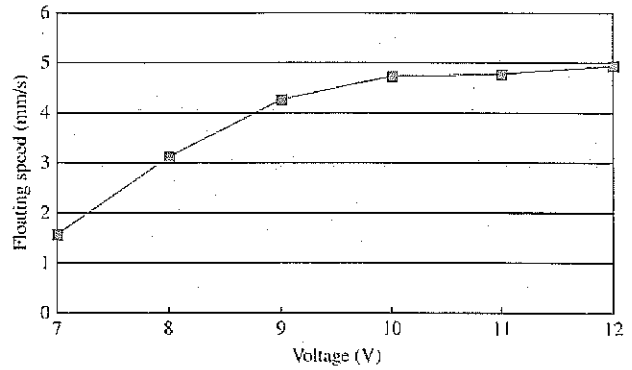


Figure 17. Theoretical floating speed of the two-ring body.

volume changed a lot. For low-voltage requirements, we chose the two-ring type for the body of the jellyfish-type microrobot.

The weight of the body can be measured at a certain time by changing the value of the input voltage. Because the floating process consists of two motions, shrinkage and comeback, we must consider the time of the comeback process, and then the average volume change per second can be calculated for the whole process. We can then obtain the theoretical floating speeds from (11), where m_1 is the mass of water squeezed out of the body and m is the total mass of the body and expelled water, as shown in Fig. 17:

$$U = \frac{Q}{A} \quad (10)$$

$$u = \frac{m_1 U}{m} \quad (11)$$

4.4 Walking Motion Mechanism

Figure 18 shows the walking mechanism. This microrobot can walk with two DOF. All the four legs have the same oscillating frequency. When walking in one direction, the phase of one leg lags that of the opposite leg by 90° . Every step cycle of the walking motion can be separated into four periods. Figure 19 shows one step cycle for forward motion. The microrobot can move a distance of d during one step cycle.

We measured the displacement of one IPMC actuator by applying different signals to simulate the theoretical crawling speed of the microrobot as shown in Fig. 20. The IPMC actuator was 20 mm long, 5 mm wide, and 0.2 mm thick. The actuator was driven by a PC equipped with a digital-to-analogue converter card, and the deflection of the IPMC was measured by a laser displacement sensor. The laser sensor was used to translate the displacement to a voltage, and then the voltages were recorded and translated to the PC using an oscilloscope.

Because the actuator was designed for use in a water tank, the relationship between the tip distance and the

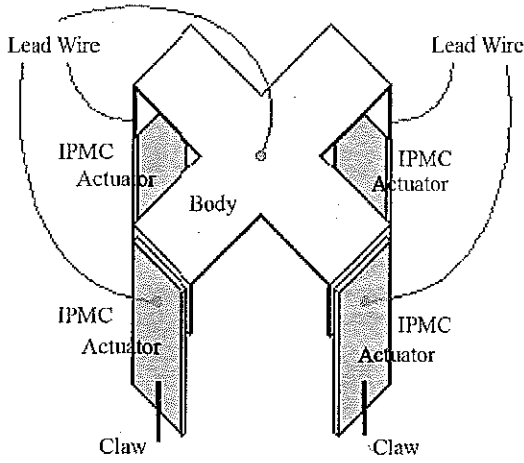


Figure 18. Microrobot structure with 2 DOF.

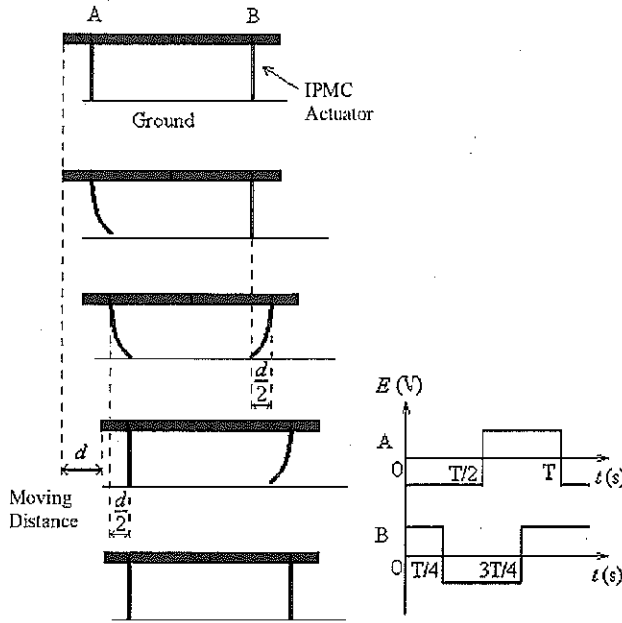


Figure 19. Microrobot walking mechanism.

laser sensor voltage was different from that relationship in air. This means that the laser sensor must first be calibrated for use in water [24]. Figure 21 shows the tip displacements of the actuator recorded experimentally for different frequencies and voltages. These results show that the tip displacement decreased as the frequency increased. Therefore, the microrobot had a top walking speed, and the theoretical walking speed could be calculated using (2).

4.5 Equivalent Cantilever Beam Modelling

The IPMC beam actuator can be modelled as a supported cantilever beam as shown in Fig. 22 [29]. When the microrobot crawling, the forces applied to one leg are shown in Fig. 23, where q is the surface tension of the IPMC actuator and F is the resultant force of friction and water

resistance to one leg. According to the cantilever beam theory, the relationship between the deformation curvature $1/\rho(x)$ and mechanical moment M is shown in (12):

$$\frac{1}{\rho(x)} = \frac{M(x)}{EI} \quad (12)$$

Where E is the elastic modulus for IPMC in hydrated conditions and I is the moment of inertia for the equivalent cantilever beam. Mechanical moment M , produced due to IPMC bending, is a function of applied forces [28, 30, 32, 33].

Also, according to curvature equation (13) of deflection curve, we can get (14):

$$\frac{1}{\rho(x)} = -\frac{\frac{d^2w}{dx^2}}{\left[1 + \left(\frac{dw}{dx}\right)^2\right]^{3/2}} \quad (13)$$

$$\frac{\frac{d^2w}{dx^2}}{\left[1 + \left(\frac{dw}{dx}\right)^2\right]^{3/2}} = -\frac{M(x)}{EI} \quad (14)$$

For the small deflection, (14) is simplified as shown in (15), which is approximately expressed:

$$\frac{d^2w}{dx^2} = -\frac{M(x)}{EI} \quad (15)$$

The tip displacement generated by the surface tension q in one direction can be defined as w_q . So, the tip displacement in two directions $d_0 = 2w_q$ can be calculated in (16):

$$d_0 = 2 \times w_q = 2 \times \frac{qx^2}{24} (-4lx + 6l^2 + x^2) = 2 \times \frac{ql^4}{8EI} = \frac{ql^4}{4EI} \quad (16)$$

The tip displacement generated by the resultant force F in one direction can be defined as w_F . So, the tip displacement in two directions $\Delta d = 2w_F$ can be calculated in (17). As a result, the resultant deflection d can be obtained from (18):

$$\Delta d = 2 \times w_F = 2 \times \left(-\frac{Fx^3}{6EI} + \frac{Flx^2}{2EI} \right) = \frac{2Fl^3}{3EI} \quad (17)$$

$$d = d_0 - \Delta d = 2 \times (w_q - w_F) = d_0 - \frac{2Fl^3}{3EI} \quad (18)$$

To calculate the w_F , the IPMC bending stiffness EI can be calculated from experiments and (19) respectively:

$$I = \frac{b \cdot h^3}{12} \quad (19)$$

The elastic modulus E for IPMC in hydrated conditions is measured with the value of about 83 MPa [25].

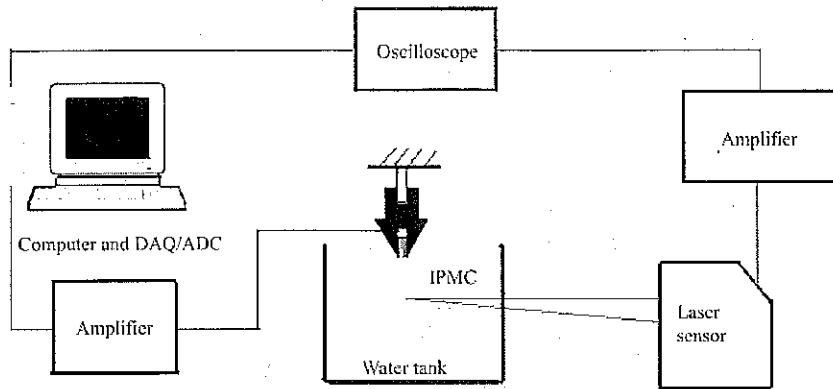


Figure 20. Displacement measuring system.

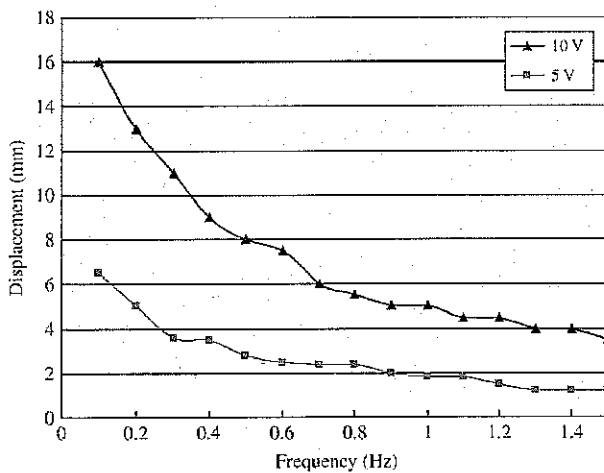


Figure 21. Tip displacements ($d_0/2$) of the IPMC actuator.

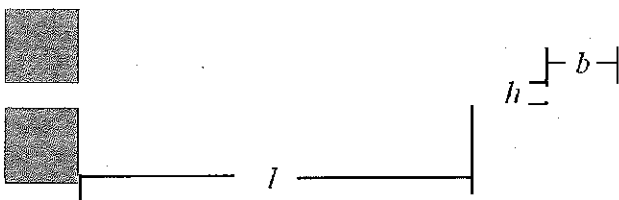


Figure 22. Equivalent cantilever beam for an IPMC actuator.

With cross dimension of $0.2 \text{ mm} \times 5 \text{ mm}$, the moment of inertia for the IPMC can be obtained about $3.3 \times 10^{-3} \text{ mm}^4$. Then the bending stiffness is calculated as 273.9 mN mm^2 . For one leg, the force F is the friction, as shown in (20):

$$F = \mu_s N \quad (20)$$

Where N is the positive pressure between the leg and the bottom of water tank, and μ_s is the static friction coefficient. According to the materials of IPMC and the hard

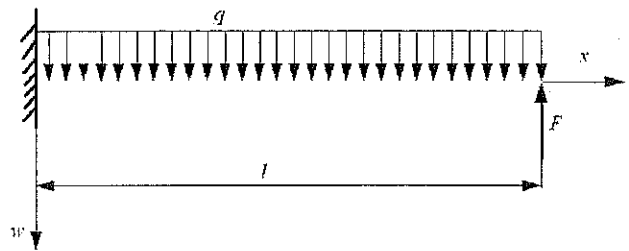


Figure 23. Forces and deflection of IPMC actuator in w direction.

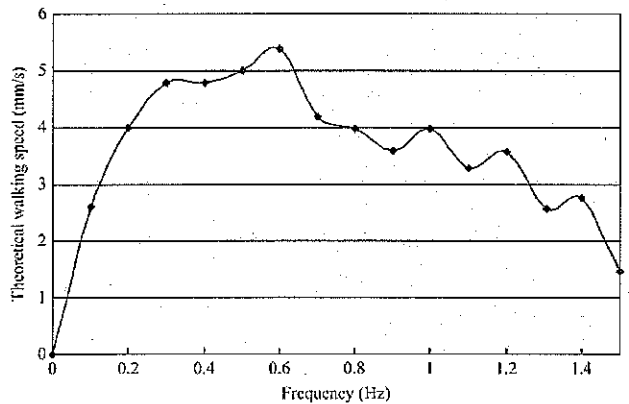


Figure 24. Theoretical walking speed of the jellyfish-type microrobot (10 V).

steel bottom, we choose $\mu_s = 0.30$ in our experiments. With the weight of 4.81 g in air and cubage of 4.6 cm^3 , the weight of the microrobot in water can be calculated as 0.21 g , $N = 0.21 \text{ g}$. So, the force F of one leg can be obtained about 0.3093 mN . With the length of leg $l = 20 \text{ mm}$, the force $F = 0.3093 \text{ mN}$, and the bending stiffness of the leg $EI = 273.9 \text{ mN mm}^2$, the displacement decreases of IPMC drivers Δd can be evaluated as 6.023 mm and the walking speeds can be calculated by (2). The simulated results are shown in Fig. 24.

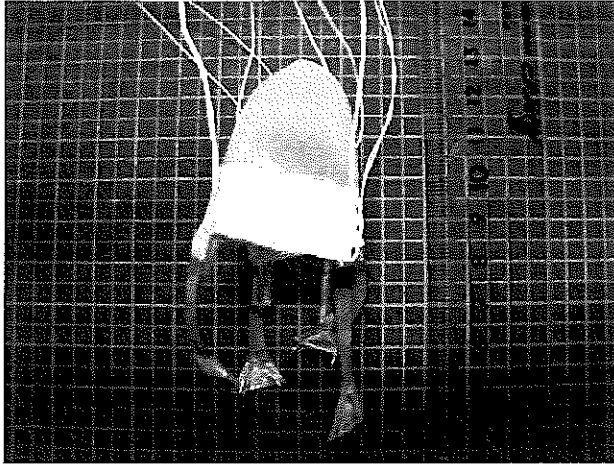


Figure 25. Prototype jellyfish-type microrobot.

Table 3
Dimensions of the Jellyfish-Type Microrobot

Width	42 mm
Height	68 mm
Weight	4.81 g
SMA actuator	20 mm (2)
IPMC actuator	5 mm × 20 mm (4)

5. Prototype Jellyfish-Type Microrobot and Experiments

5.1 Prototype Microrobot

A prototype jellyfish-type microrobot was constructed based on the results of the experiments described earlier [27]. Figure 25 shows the prototype, and Table 3 lists its dimensions. It had four IPMC actuators fixed on a two-ring type body [31]. The control signals were transmitted by enamel-covered wires 300 mm long with a copper diameter of 0.03 mm. The wires were soft enough that the resistance could be ignored.

5.2 Floating Experiment

The robot was placed in a water tank as shown in Fig. 26. To obtain a high floating speed, we chose the duty cycle of the input voltage to be 65% at a frequency of 1 Hz. We then measured the average speeds of the robot with different voltages (1–12 V) for a floating distance of 20 mm; the results are shown in Fig. 27. The floating speed increased as the voltage increased. When the input voltage was higher than 10 V, the floating speed was 6 mm/s. When the input voltage was cut off, the microrobot stopped floating upward and immediately started to sink. Therefore, the jellyfish-type microrobot had a better floating performance than the eight-legged one. The experimental results are almost the same as the theoretical results as shown in Fig. 28.

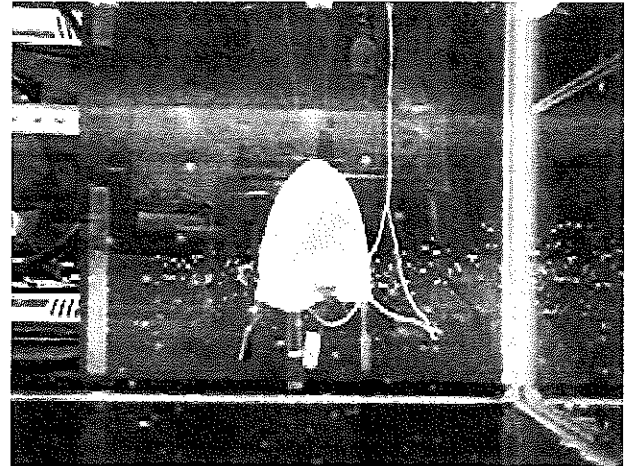


Figure 26. Floating motion of the jellyfish-type microrobot.

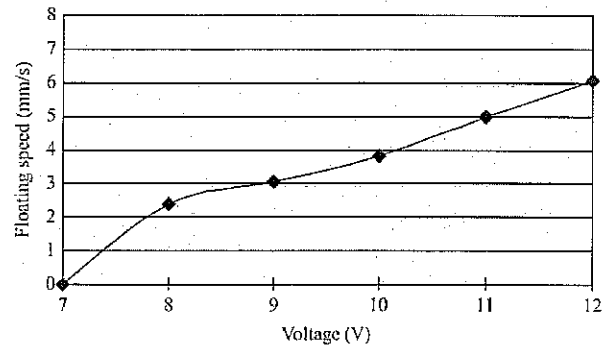


Figure 27. Experimental floating speed results.

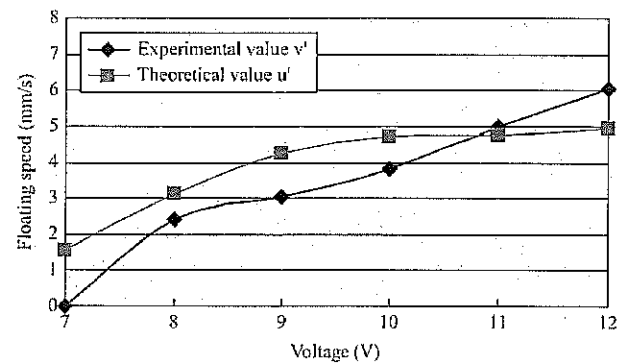


Figure 28. Relationship between theoretical and experimental values.

5.3 Walking Experiment

We conducted an underwater experiment on a plastic surface, as shown in Fig. 29, to evaluate the walking motion of the jellyfish-type microrobot. We recorded the times to walk a distance of 50 mm for control signals of different voltage and frequency. We repeated the experiment with

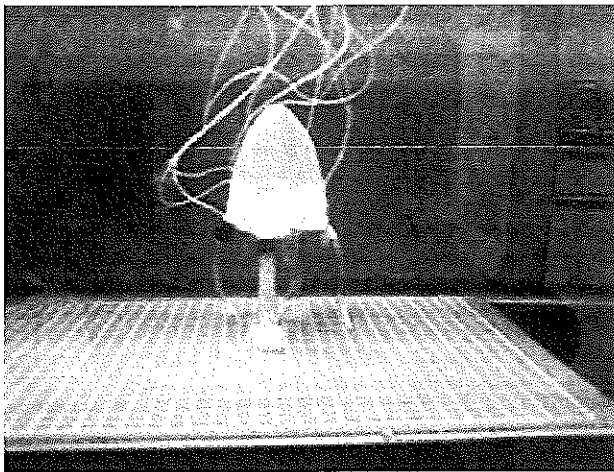


Figure 29. Walking motion of the jellyfish-type micro-robot.

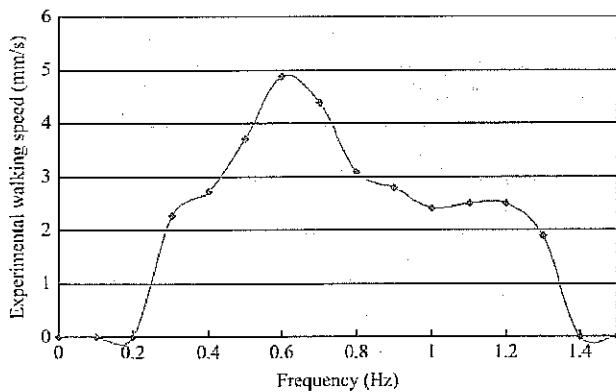


Figure 30. Experimental walking speed results (10 V).

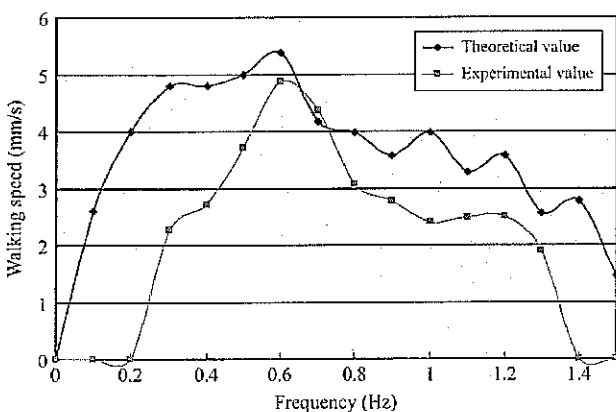


Figure 31. Relationship between theoretical and experimental speeds (10 V).

each set of control signals 10 times so we could determine the average speed on the flat surface; Fig. 30 shows the results. The displacement of the IPMC actuator would be less in real applications due to loading, slippage, and short response time at high frequencies. Therefore, some

differences between the theoretical and experimental results exist as shown in Fig. 31.

6. Conclusions

To resolve the problem of the asymmetry in previous six-legged microrobots, we proposed a new type of underwater microrobot with eight IPMC actuators distributed symmetrically around the microrobot's centre of symmetry. We evaluated the walking, rotating, and floating mechanisms of this proposed robot. We also constructed a prototype of the eight-legged microrobot and conducted experiments to measure its walking speed and angular velocity with and without payloads. Its walking and rotating speeds were faster than those of the previous six-legged version. We also made the microrobot dive and surface by electrolysis of the water around the IPMC surface. Controlling the electrolysis process and thus the buoyancy of the microrobot was difficult, so the vertical motion of the device could not be controlled very well.

To create a compact structure with efficient locomotion characteristics, we proposed a jellyfish-type microrobot to imitate the way a jellyfish moves up or down in water. We evaluated the characteristics of three types of microrobot bodies experimentally. We chose the two-ring type and calculated its theoretical floating speed. We then analysed the walking mechanism of the jellyfish-type microrobot and calculated its theoretical walking speed. Finally, we developed a prototype of the jellyfish-type microrobot and measured its actual floating and walking speeds. The floating motion of the last prototype was superior to the previous model.

Acknowledgement

This research is supported by Kagawa University Characteristic Prior Research Fund 2010.

References

- [1] B. Kim, D. Kim, J. Jung, & J. Park, A biomimetic undulatory tadpole robot using ionic polymer-metal composite actuators, *Journal of Smart Material and Structures*, 14, 2005, 1579-1585.
- [2] S.T. McGovern, G.M. Spinks, B. Xil, G. Alici, V. Truong, & G.G. Wallace, Fast bender actuators for fish-like aquatic robots, *Proceedings of SPIE*, 6927, 2008, 69271L.
- [3] B. Behkam & M. Sitti, Design methodology for biomimetic propulsion of miniature swimming robots, *Journal of Dynamic Systems, Measurement, and Control*, 128(1), 2006, 36-43.
- [4] W. Zhang, S. Guo, & K. Asaka, A new type of hybrid fish-like microrobot, *International Journal of Automation and Computing*, 3(4), 2006, 358-365.
- [5] Z. Wang, G. Hang, J. Li, Y. Wang, & K. Xiao, A micro-robot fish with embedded SMA wire actuated flexible biomimetic fin, *Journal of Sensors and Actuators A*, 144, 2008, 354-360.
- [6] S. Heo, T. Wiguna, H. Park, & N. Goo, Effect of an artificial caudal fin on the performance of a biomimetic fish robot propelled by piezoelectric actuators, *Journal of Bionic Engineering*, 4(3), 2007, 151-158.
- [7] S. Guo, L. Shi, & K. Asaka, IPMC actuator-based an underwater microrobot with 8 legs, *Proceedings of 2008 IEEE International Conference on Mechatronics and Automation*, Japan, 2008, 551-556.
- [8] S. Kim, I. Lee, & Y. Kim, Performance enhancement of IPMC actuator by plasma surface treatment, *Journal of Smart Material and Structures*, 16, 2007, N8-N11.

- [9] S. Lee & K. Kim, Muscle-like linear actuator using an ionic polymer-metal composite and its actuation characteristics, *Journal of Smart Structures and Materials: Electroactive Polymer Actuators and Devices (EAPAD)*, *Proceedings of SPIE*, 6168, 2006, 616820.
- [10] D. Dogruer, R. Tiwari, & K. Harvesters, Ionic polymer metal composites as energy harvesters, *Journal of Electroactive Polymer Actuators and Devices (EAPAD)*, *Proceedings of SPIE*, 6524, 2007, 65241C.
- [11] S. Liu, M. Lin, & Q. Zhang, Extensional ionic polymer conductor composite actuators with ionic liquids, *Journal of Electroactive Polymer Actuators and Devices (EAPAD)*, *Proceedings of SPIE*, 6927, 2008, 69270H.
- [12] H. Nakadoi, A. Sera, M. Yamakita, K. Asaka, Z. Luo, & K. Ito, Integrated actuator-sensor system on patterned IPMC film: Consideration of electric interference, *Proceedings of the 2007 4th IEEE International Conference on Mechatronics*, Kumamoto, Japan, 2007, 4280007.
- [13] A. Punning, M. Kruusmaa, & A. Aabloo, Surface resistance experiments with IPMC sensors and actuators, *Journal of Sensors and Actuators A*, 133, 2007, 200-209.
- [14] S. Guo, L. Shi, & K. Asaka, IPMC actuator-sensor based a biomimetic underwater microrobot with 8 legs, *Proceedings of the IEEE International Conference on Automation and Logistics*, China, 2008, 2495-2500.
- [15] S. Guo, L. Shi, K. Asaka, & L. Li, Experiments and characteristics analysis of a bio-inspired underwater microrobot, *Proceedings of the 2009 IEEE International Conference on Mechatronics and Automation*, China, 2009, 3330-3335.
- [16] X. Ye, Y. Su, S. Guo, & L. Wang, Design and realization of a remote control centimeter-scale robotic fish, *Proceedings of the 2008 IEEE/ASME International Conference on Advanced Intelligent Mechatronics*, China, 2008, 25-30.
- [17] N. Kamamichi, M. Yamakita, K. Asaka, & Z. Luo, A snake-like swimming robot using IPMC actuator/sensor, *Proceedings of the 2006 IEEE International Conference on Robotics and Automation*, Orlando, United States, 2006, 1812-1817.
- [18] J. Jung, B. Kim, Y. Tak, & J.-O. Park, Undulatory Tadpole Robot (TadRob) using ionic polymer metal composite (IPMC) actuator, *Proceedings of the IEEE/RSJ International Conference on Intelligent Robots and Systems*, Las Vegas, United States, 2003, 2133-2138.
- [19] S. Guo, Y. Okuda, & K. Asaka, Development of a novel type of underwater micro biped robot with multi DOF, *Proceedings of the 14th of International Offshore and Polar Engineering Conference*, Toulon, France, II, 2004, 284-289.
- [20] S. Guo, Y. Okuda, W. Zhang, X. Ye, & K. Asaka, The development of a hybrid underwater micro biped robot, *Journal of Applied Bionics and Biomechanics*, 3(3), 2006, 143-150.
- [21] N. Kamamichi, Y. Kaneda, M. Yamakita, K. Asaka, & Z.W. Luo, Biped walking of passive dynamic walker with IPMC linear actuator, *SICE Annual Conference*, Fukui, 2003, 212-217.
- [22] W. Zhang, S. Guo, & K. Asaka, Development of a novel type of an underwater microrobot with biomimetic locomotion, *Journal of Applied Bionics and Biomechanics*, 3(3), 2006, 245-252.
- [23] W. Zhang, S. Guo, & K. Asaka, A tripod biomimetic underwater microrobots utilizing ICPF actuators, *Proceedings of the 2006 IEEE/RSJ International Conference on Intelligent Robots and Systems*, Beijing, China, 2006, 2418-2423.
- [24] W. Zhang, S. Guo, & K. Asaka, Characteristics analysis of a biomimetic underwater walking microrobot, *Proceedings of the 2006 IEEE International Conference on Robotics and Biomimetics*, Kunming, China, 2006, 1600-1605.
- [25] I. Park, S. Kim, D. Kim, & K. Kim, The mechanical properties of ionic polymer-metal composites, *Journal of Electroactive Polymer Actuators and Devices (EAPAD)*, *Proceedings of SPIE*, 6524, 2007, 65241R.
- [26] W. Yim, J. Lee, & K.J. Kim, An artificial muscle actuator for biomimetic underwater propulsors, *Journal of Bioinspiration and Biomimetics*, 2, 2007, S31-S41.
- [27] S. Guo, L. Shi, X. Ye, & L. Li, A new jellyfish type of underwater microrobot, *Proceedings of the 2007 IEEE International Conference on Mechatronics and Automation*, China, 2007, 509-514.
- [28] P. Brunetto, L. Fortuna, S. Graziani, & S. Strazzeri, A model of ionic polymer-metal composite actuators in underwater operations, *Journal of Smart Material and Structures*, 17, 2008, 25-29.
- [29] H. Cilingir, Y. Menceloglu, & M. Papila, The effect of IPMC parameters in electromechanical coefficient based on equivalent beam theory, *Journal of Electroactive Polymer Actuators and Devices (EAPAD)*, *Proceedings of SPIE*, 6927, 2008, 69270L.
- [30] D. Pugal, H. Kasemagi, M. Kruusmaa, & A. Aabloo, An advanced finite element model of IPMC, *Journal of Electroactive Polymer Actuators and Devices (EAPAD)*, *Proceedings of SPIE*, 6927, 2008, 692711.
- [31] S. Yeom & I. Oh, A biomimetic jellyfish robot based on ionic polymer metal composite actuators, *Journal of Smart Materials and Structures*, 18, 2009, 085002.
- [32] B. Stoimenov, J. Rossiter, T. Mukai, & K. Asaka, Frequency response of anisotropic ionic polymer metal composite (IPMC) transducers, *Journal of Electroactive Polymer Actuators and Devices (EAPAD)*, *Proceedings of SPIE*, 6927, 2008, 69270K.
- [33] E. Mbermo, Z. Chen, S. Shataru, & X. Tan, Modeling of biomimetic robotic fish propelled by an ionic polymer-metal composite actuator, *Proceedings of the IEEE International Conference on Robotics and Automation*, Pasadena, United States, 2008, 689-694.

Biographies



Liwei Shi received his B.S. degree in Mechanical Engineering from Harbin Engineering University, China, in 2006, and the M.S. degree in Intelligent Machine System from Kagawa University, Japan, in 2009. Currently, he is a Ph.D. candidate in Kagawa University, Japan. He researches on underwater microrobot utilizing artificial muscles, such as IPMC (ionic polymer metal composite) actuators for industry and biomedical applications. His current research interests include legged microrobots and jellyfish-type microrobot. He has published about eight refereed journal and conference papers in recent 2 years. He is an IEEE student member.



Shuziang Guo (S'93-M'95-SM'03) received the B.S. and the M.S. degrees in Mechanical Engineering from the Changchun Institute of Optics and Fine Mechanics, Changchun, China, in 1983 and 1986, respectively, and the Ph.D. degree in Mechano-Informatics and Systems from Nagoya University, Nagoya, Japan, in 1995. In 1995, he was a faculty member at Mie University, Mie, Japan and in 1998 at Kagawa University, Kagawa, Japan. Currently, he is a professor with the Department of Intelligent Mechanical System Engineering at Kagawa University. He has published about 270 refereed journal and conference papers. His current research interests include microrobotics and mechatronics, microrobotics system for minimal invasive surgery, microcatheter system, micropump, and smart material (SMA, ICPF) based on actuators. He received

research awards from the Tokai Section of the Japan Society of Mechanical Engineers (JSME), the Tokai Science and Technology Foundation, the Best Paper Award of the IS International Conference, Best Paper award of the 2003 International Conference on Control Science and Technology, and Best Conference Paper Award of IEEE ROBIO2004, in 1997, 1998, 2000, 2003, and 2004, respectively.



Kinji Asaka received his Ph.D. degree in Science from Kyoto University in 1991. He is currently a group leader of the Artificial Cell Research Group, Research Institute for Cell Engineering of National Institute of Advanced Industrial Science and Technology (AIST). His current research interests include interfacial electrochemistry and polymer actuators. He is a member of the Society of

Polymer Science, Japan and The Society of Instrument and Control and Engineers.